Facile Electron Transfer during Formation of Cluster X and Kinetic Competence of X for Tyrosyl Radical Production in Protein R2 of Ribonucleotide Reductase from Mouse†

Danny Yun,‡ Carsten Krebs,⊥ Govind P. Gupta,⊥ David F. Iwig,‡ Boi Hanh Huynh,⊥ and J. Martin Bollinger, Jr.*,‡

Department of Biochemistry and Molecular Biology, Pennsylvania State University, University Park, Pennsylvania 16802, and Department of Physics, Emory University, Atlanta, Georgia 30322

Received September 17, 2001; Revised Manuscript Received November 13, 2001

ABSTRACT: The kinetics and mechanism of formation of the tyrosyl radical and μ-(oxo)diiron(III) cluster in the R2 subunit of ribonucleotide reductase from mouse have been examined by stopped-flow absorption and freeze-quench electron paramagnetic resonance and Mössbauer spectroscopies. The reaction comprises (1) acquisition of Fe(II) ions by the R2 apo protein, (2) activation of dioxygen at the resulting carboxylate-bridged diiron(II) cluster to form oxidized intermediate diiron species, and (3) univalent oxidation of Y177 by one of these intermediates to form the stable radical, with concomitant or subsequent formation of the adjacent μ-(oxo)diiron(III) cluster. The data establish that an oxidized diiron intermediate spectroscopically similar to the well-characterized, formally Fe(III)Fe(IV) cluster X from the reaction of the *Escherichia coli* R2 protein precedes the Y177 radical in the reaction sequence and is probably the Y177 oxidant. As formation of the X intermediate (1) requires transfer of an "extra" reducing equivalent to the buried diiron cluster following the addition of dioxygen and (2) is observed to be rapid relative to other steps in the reaction, the present data indicate that the transfer of this reducing equivalent is not rate-limiting for Y177 radical formation, in contrast to what was previously proposed (Schmidt, P. P., Rova, U., Katterle, B., Thelander, L., and Gräslund, A. (1998) *J. Biol. Chem. 273*, 21463−21472). Indeed, the formation of X ($k_{obs} = 13 \pm 3$ s^{-1} at 5 °C and 0.95 mM O_2) and the decay of the intermediate to give the Y177 radical ($k_{obs} = 5 \pm 2$ s^{-1}) are both considerably faster than the formation of the reactive Fe(II)−R2 complex from the apo protein and $Fe(II)_{aq}$ ($k_{obs} = 0.29 \pm 0.03$ s^{-1}), which is the slowest step overall. The conclusions that cluster X is an intermediate in Y177 radical formation and that transfer of the reducing equivalent is relatively facile imply that the mouse R2 and *E. coli* R2 reactions are mechanistically similar.

The essential metallocofactor of class I ribonucleotide reductase is a μ-(oxo)-μ-(carboxylato)diiron(III) cluster adjacent to a stable tyrosyl radical (*1*−*3*). This cofactor assembles in a spontaneous reaction that comprises the acquisition of Fe(II) ions by the R2 apo protein, activation of O_2 at the resulting diiron(II) cluster, and univalent oxidation of a tyrosine residue to produce the stable radical (*4*). In the past decade, the cofactor assembly reactions of the R2 proteins from *Escherichia coli* (*3*, *5*−*8*), mouse (*9*−*12*), and (most recently) yeast (*13*, *14*) have been investigated. The *E. coli* R2 reaction has been most thoroughly described, and kinetic and spectroscopic data indicate that it proceeds according to Scheme 1. Acquisition of Fe(II) ions to form the O_2-reactive Fe(II)−R2 complex (step A) is rate-limiting for formation of oxidized intermediates and has the kinetic characteristics of a unimolecular (conformational) change by the protein (*15*, *16*). Prior incubation of Fe(II) and apo R2 in the absence of O_2 followed by initiation of the reaction by mixing with O_2 allows the subsequent faster steps beginning with addition of O_2 to the diiron(II) cluster (step B) to be interrogated (*7*, *16*). Upon addition of O_2, multiple nuclear and electronic rearrangements (steps C) rapidly ensue, and the first intermediate state that has been definitively demonstrated contains the formally Fe(III)Fe(IV) cluster X (*5*, *7*, *17*−*19*). Characterization of X by ENDOR[1] and EXAFS spectroscopies has suggested that the O−O bond of O_2 has been cleaved, with one of the O atoms having become the μ-oxo and the second having become coordinated to the Fe(III) ion as hydroxide or water (*20*−*23*). In this first isolable intermediate state, the second oxidizing equivalent of the initial diiron(II)−O_2 adduct is stored as the cation radical of the near-surface tryptophan 48 (W48) (*7*, *8*, *24*). At all routinely accessible reactant

† This work was supported by NIH Grants GM55365 to J.M.B. and GM58778 to B.H.H.

* To whom correspondence should be addressed. Phone: (814) 863-5707. Fax: (814) 863-7024. E-mail: jmb21@psu.edu.

‡ Pennsylvania State University.

⊥ Emory University.

[1] Abbreviations: ENDOR, electron nuclear double resonance; EXAFS, extended X-ray absorption fine structure; EPR, electron paramagnetic resonance; 2-ME, 2-mercaptoethanol; $W^{+\bullet}$, tryptophan 48 cation radical; k_{obs}, observed apparent first-order rate constant; Y177•, tyrosyl radical in mouse R2; Y122•, tyrosyl radical in *E. coli* R2; IPTG, isopropylthiogalactopyranoside; PMSF, phenylmethysulfonylfluoride; Tris, tris[hydroxymethyl]aminomethane; HEPES, 4-[2-hydroxyethyl]-1-piperazineethanesulfonic acid; PCR, polymerase chain reaction; SDS−PAGE, sodium dodecyl sulfate−polyacrylamide gel electrophoresis.

10.1021/bi011797p CCC: $22.00
Published on Web 12/20/2001

Scheme 1: Mechanism of cofactor assembly in the R2 subunit of ribonucleotide reductase from *E. coli* as carried out in the presence of reductant.

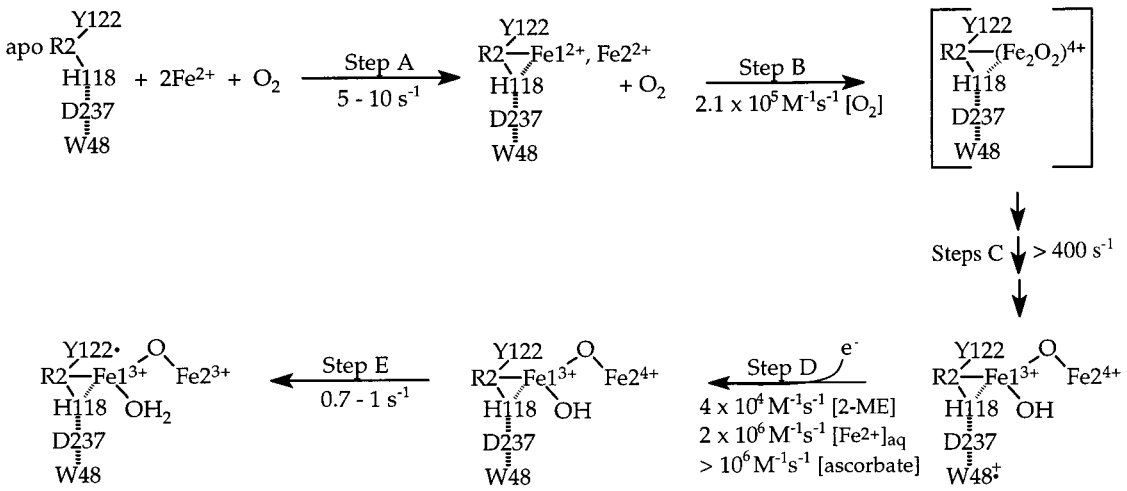

concentrations, combination of the Fe(II)−R2 complex and O_2 (step B) is slower than the sequence of steps (C) leading to the X−$W^{+\bullet}$ state (*7*). For this reason, the addition of O_2 and the subsequent oxidation of W48 are kinetically unresolved. However, simulations of the kinetics of $W^{+\bullet}$ formation have allowed a lower limit of 400 s^{-1} to be set for the rate constant of the W48-oxidation step (*7*). In the presence of a sufficiently high concentration of an appropriate reductant (e.g., 2-mercaptoethanol [2-ME], excess Fe(II), or ascorbate), the $W^{+\bullet}$ can be reduced (step D) sufficiently rapidly that it does not accumulate (*7*, *15*, *24*). Reduction of the $W^{+\bullet}$ completes the two-step, W48-mediated shuttling of a reducing equivalent from an exogenous reductant to the buried, reacting diiron center. The intermediate state that results contains only cluster X. The slowest step in the reaction (as carried out in the presence of a facile reductant) is the last step, oxidation of Y122 by X to form the Y122 radical and the product μ-(oxo)diiron(III) cluster (step E, 0.7−1 s^{-1}) (*5*, *15*).

The results of recent kinetics and mutagenesis experiments on the R2 protein from mouse (expressed in *E. coli*) would suggest that its reaction differs markedly in kinetic details, if not more profoundly in mechanistic pathway, from the reaction of *E. coli* R2 (*11*). Schmidt et al. reported that tyrosyl radical (Y177•) formation in mouse R2 is slower (k_{obs} = 0.14 ± 0.03 s^{-1} at 5 °C as compared to 0.7−1 s^{-1} in *E. coli* R2) and proceeds without accumulation of a cognate of X. They further reported that Y177• forms with nearly identical kinetics whether Fe(II) and apo R2 are preincubated prior to initiation of the reaction with O_2 or the apo protein is mixed in the presence of O_2 with Fe(II). On this basis (and under the presumption that they had successfully generated the reactive Fe(II)−R2 complex in their anoxic preincubation of apo R2 and Fe(II)), they discounted the possibility that acquisition of Fe(II) is so slow as to prevent accumulation of oxidized intermediates (e.g., X). They then showed that Y177• formation in R2 variants with either W103 (the counterpart of the electron-shuttling W48 in *E. coli* R2) substituted with Y or D266 (the residue to which W103 is hydrogen-bonded) substituted with A is ~20-fold slower than in the reaction of the wild-type protein under identical conditions. To rationalize both the failure of an X cognate to accumulate in the wild-type R2 reaction and the slowing of Y177• formation upon substitution of residues in the network that mediates transfer of the "extra" reducing equivalent, they proposed that this transfer step is rate-limiting for formation of Y177•. This hypothesis ascribes to the transfer step in the mouse R2 reaction a rate constant 3600-fold less than the *lower limit* set for the rate constant of the cognate step in the *E. coli* R2 reaction (*7*). Moreover, the authors argued that a "mouse X" species that they did detect in small quantities only under certain reaction conditions was not on the pathway to Y177•, hinting that the tyrosyl radical in mouse R2 is generated by an intermediate distinct from that previously shown to generate the radical in the homologous *E. coli* protein (*11*). We reasoned that further delineation of these apparent kinetic/mechanistic differences between the *E. coli* R2 and mouse R2 reactions and elucidation of the structural basis for the differences might provide insight into the control of this potent reactivity by the R2 proteins. We, therefore, undertook a re-examination of the mouse R2 reaction.

MATERIALS AND METHODS

Materials. The plasmid pET3a with the mouse R2 gene (*25*) was generously provided by Professor Harvey Rubin (University of Pennsylvania). Culture media components (yeast extract and tryptone) were purchased from Marcor Development Corporation (Hackensack, NJ). Isopropyl β-D-thiogalactopyranoside (IPTG) was purchased from Biosynth International (Naperville, IL). Spectinomycin dihydrochloride, phenylmethylsulfonyl fluoride (PMSF), streptomycin sulfate, Trizma base (Tris), and 1,10-phenanthroline were purchased from Sigma (St. Louis, MO). Ampicillin was purchased from IBI (Shelton, CT). Glycerol, ammonium sulfate, and sodium chloride were purchased from EM Science (Gibbstown, NJ). Enzyme grade 4-(2-hydroxyethyl)-1-piperazineethanesulfonic acid (HEPES) was purchased from FisherBiotech (Pittsburgh, PA). Oligonucleotide primers were purchased from Gibco/BRL (Grand Island, NY). Restriction enzymes and reagents for the polymerase chain reaction (PCR) were purchased from New England Biolabs (Beverly, MA). T4 DNA ligase was purchased from Roche (Indianapolis, IN). DNA sequence determination was performed by the Nucleic Acid Facility of the Pennsylvania State University Biotechnology Institute. BL21(DE3) and pET

vectors were purchased from Novagen (Madison, WI). The plasmid pSJS1240 (*26*) was a kind gift from Professor Craig Cameron (Pennsylvania State University).

Preparation of Vectors and Strains for Overexpression of R2 and R2−Y177F. Plasmid pMR2, which contains the mouse R2 gene inserted into the pET22b expression vector, was constructed as follows. The mouse R2 gene was amplified by PCR with primers 1 (5′-GGA GAT ATA **CAT ATG** CTC TCC GTC CGC-3′ with *NdeI* site shown in boldface) and 2 (5′-GTT AGC AGC **CTC GAG** TTA GAA GTC AGC ATC CAA GG-3′ with *XhoI* shown in boldface) and pET3a as template. The 1197 basepair PCR fragment was purified by agarose gel electrophoresis, extracted from the gel by using the Qiagen (Valencia, CA) QiaQuick system as instructed by the manufacturer, restricted with *NdeI* and *XhoI*, repurified as before, and ligated with pET22b that had been digested with the same enzymes and gel purified. The sequence of the coding region of the vector was verified. BL21(DE3) cells were transformed with both pMR2 and pSJS1240 plasmids. The latter encodes for rare tRNAs for arginine and isoleucine and confers resistance to spectinomycin (*26*).

The Y177F substitution (TAC to TTC, underlined) was introduced by PCR by using primer 3 (5′-A ATT G**CC ATG G**AA AAC ATA CAC TCT GAA ATG TTC AGT CTC C-3′ with *NcoI* restriction site in boldface), primer 2 above, and pMR2 as template. The 687 basepair fragment was gel purified, restricted with *NcoI* and *XhoI*, repurified, and ligated with *NcoI*/*XhoI*-restricted pET22b to give pMR2−Y177F. The sequence of the entire coding region was verified. BL21-(DE3) cells were transformed with the pMR2−Y177F and pSJS1240 plasmids.

Expression and Purification of apo R2 and apo R2−Y177F. BL21(DE3) cells transformed with pMR2 and pSJS1240 or with pMR2−Y177F and pSJS1240 were grown at 37 °C in rich medium containing 35 g/L tryptone, 20 g/L yeast extract, 5 g/L NaCl, 0.15 g/L ampicillin, and 0.05 g/L spectinomycin. Exponentially growing cultures with OD_{600} of 0.8−1 were treated with 0.5 mM 1,10-phenanthroline, incubated an additional fifteen minutes, and then induced to express R2 by addition of IPTG to 0.5 mM. Cultures were grown an additional 1.5 h after induction and then chilled on ice. Cells were harvested by centrifugation at 3800*g* for 10 min. The cell pellet was washed with cold 25 mM Tris HCl (pH 7.4) containing 70 mM NaCl and 4 mM KCl prior to being frozen in liquid N_2 and stored at −80 ° C. A typical yield was ∼5 g of wet cell paste/L of culture.

In a typical purification, 60 g of wet cell paste was resuspended in buffer A [50 mM Tris HCl (pH 7.6) and 10% (v/v) glycerol] containing 0.25 mM PMSF and 1 mM 1,10-phenanthroline. Lysis was accomplished by passage through a French pressure cell at 16 000 psi. The crude lysate was centrifuged at 13 900*g* for 10 min. Streptomycin sulfate was added to a final concentration of 1% (w/v) to precipitate ribosomal proteins and nucleic acids. The precipitate was removed by centrifugation at 13 900*g* for 10 min. Solid ammonium sulfate was added to the supernatant to 40% of saturation (0.243 g/mL). The precipitate was isolated by centrifugation at 13 900*g* for 10 min. The pellet was dissolved in buffer A (1 mL/g wet cell pellet) containing 0.25 mM PMSF and 1 mM 1,10-phenanthroline. After a 4 h dialysis against 4 L of buffer A, the solution was diluted by addition of an equal volume of buffer A and then applied to a 600 mL Q-Sepharose (Amersham-Pharmacia, Cleveland, OH) column in buffer A. The protein was eluted with a linear gradient of 120−240 mM NaCl in buffer A. The fractions with R2 protein (assessed in initial purifications by SDS−PAGE) were pooled and concentrated to approximately 10 mg/mL in an Amicon (Beverly, MA) ultrafiltration cell with a YM30 membrane. The protein was dialyzed against 2 L of buffer C [100 mM HEPES (pH 7.6) and 10% (v/v) glycerol] for 4 h to remove the NaCl and exchange the buffer. The protein was concentrated to approximately 35 mg/mL in a Centriprep 30 Concentrator (Amicon), flash-frozen in liquid N_2, and stored at −80 °C. SDS−PAGE with coomassie staining was used to estimate the purity of the protein. A typical yield was 220 mg of protein from 60 g of wet cell paste.

Determination of Protein Concentration. An effective molar absorptivity, $\epsilon_{280-310}$, of 124 000 M^{-1} cm^{-1} has been reported for the mouse R2 dimer (*27*). The intent of subtraction of the absorbance at 310 nm (A_{310}) from that at 280 nm (A_{280}) is to provide an absorbance reading that is independent of the Fe and Y177• content of the protein and, thereby, to permit routine spectrophotometric determination of [R2] in samples with different cofactor contents (*27*). Mouse R2 isolated according to our procedure has very little (essentially undetectable) Fe and Y177•, and consequently, A_{310} is almost negligible (2−4%) with respect to A_{280}. Therefore, uncorrected values of A_{280} were used to determine R2 concentrations according to the molar absorptivity of 124 000 M^{-1} cm^{-1} for the dimer. The effect of correcting these values by subtraction of A_{310} would have been to decrease the measured protein concentration by less than 4% (in all cases) and, thereby, to increase measured Fe/R2 and Y177•/R2 stoichiometries by the same small percentage.

Determination of Limiting Fe(II)/R2, Y177•/R2, and Fe(II)/Y177• Stoichiometries for the Reaction. Air-saturated solutions of the apo protein (90−160 μM) were titrated at ambient temperature (22 ± 2 °C) with Fe(II) stock solutions of known concentration. After each addition, spectra were recorded every minute for 3 min on a Hewlett-Packard HP8453 spectrophotometer. The drop-line corrected absorbance at 416 nm [$A_{416} - (A_{410} + A_{422})/2$] (*15*) was used to determine when the titration had reached completion (see Figure 2). At least three additions were made after completion to permit accurate assessment of the equivalence point, which was determined by the point of intersection of linear fits to the two phases of the $A_{416} - (A_{410} + A_{422})/2$ versus Fe(II)/R2 plots (see inset to Figure 2). The dropline-corrected molar absorptivity, $\epsilon_{416} - (\epsilon_{410} + \epsilon_{422})/2$, for the Y177 radical was determined, as previously described for the Y122• in *E. coli* R2 (*15*), by determining [Y177•] for several samples directly by EPR and plotting $A_{416} - (A_{410} + A_{422})/2$ for these samples versus [Y177•] (see Figure S1, Supporting Information). The slope of this plot gave $\epsilon_{416} - (\epsilon_{410} + \epsilon_{422})/2$ as 463 ± 20 M^{-1} cm^{-1}. In the above titrations, [Y177•] was determined spectrophotometrically by using this effective molar absorptivity.

Preparation of the Fe(II)−R2 Complex. Solutions of apo R2 or apo R2−Y177F were rendered free of oxygen on a vacuum/gas manifold and then mixed with Fe(II) in an anoxic chamber (MBraun), as previously described (*28*). The ^{57}Fe-(II) stock solution used to prepare Mössbauer samples was

prepared by dissolution of the metal in 1 M H_2SO_4, as previously described (*15*).

Stopped-Flow Spectrophotometry. Stopped-flow absorption experiments were carried out with an Applied Photophysics SX.18MV stopped-flow apparatus equipped with a diode array detector and housed in the anoxic chamber. Constant temperature was ensured with a Lauda K-4/R circulating water bath. Specifics of reaction conditions are given in the legend to Figure 3.

Freeze-Quench EPR and Mössbauer Experiments. The apparatus and procedures for preparation of freeze-quenched samples have been described (*6*, *18*). The EPR and Mössbauer spectrometers have been described (*7*, *18*). Specific sample attributes and spectrometer settings are given in the legends to Figures 4−6.

RESULTS AND DISCUSSION

Expression and Purification of Mouse R2. SDS−PAGE analysis of total extracts of BL21(DE3)-pMR2 harvested from rich medium after a 1.5 h induction at 37 °C with 0.5 mM IPTG revealed a band at the correct molecular weight (∼45 kDa) for mouse R2. However, the level of expression was low as compared to those that we have obtained in overproduction of proteins from *E. coli* and other bacteria. During attempts to understand why expression was poor, several occurrences of the uncommonly used (by *E. coli*) AGG (5) and AGA (6) codons for Arg were noted in the mouse R2 gene sequence. In case the presence of these codons might limit expression, the strain was transformed with the plasmid pSJS1240, which confers spectinomycin resistance and encodes tRNAs for the AG(A,G) codons for Arg and the rare ATA codon for Ile (*26*). From SDS−PAGE analysis of induced BL21(DE3)-pMR2 and BL21(DE3)-pMR2/pSJS1240 and from comparison of yields of purified protein, it was tentatively concluded that the presence of this plasmid does augment R2 production somewhat (∼1.5−2-fold). It is noted, however, that the rigorous quantitation necessary to prove this conclusion has not been performed.

Purification of mouse R2 from extracts of BL21(DE3)-pMR2/pSJS1240 primarily by anion exchange chromatography typically yielded 2−5 mg of protein/g of wet cell paste. SDS−PAGE analysis of column fractions from the chromatography step and, to a lesser extent, the final purified protein revealed a triplet banding pattern in the molecular weight range of ∼40−45 kDa (Figure 1). This pattern has been observed by other investigators and attributed to proteolysis of R2 (*27*, *29*). In a typical preparation, the three bands contribute >95% of the coomassie staining intensity and are present with a distribution of approximately 0.75/0.20/0.05, with the highest molecular weight species, which is presumably full-length R2, the most prevalent. The sample of wild-type R2 analyzed for Figure 1 (lanes 4 and 5) had an unusually high extent of proteolysis and was chosen in order to clearly depict the banding pattern.

Determination of Limiting Fe(II)/R2, Y177•/R2, and Fe(II)/Y177• Stoichiometries for the Reaction. Addition of Fe(II) in the presence of O_2 to the mouse R2 apo protein results in the development of the 416 nm peak of the Y177• and the ∼325 and ∼365 nm features of the μ-(oxo)diiron(III) cluster (Figure 2). As previously reported (*27*), the 416 nm feature is considerably less sharp than the corresponding feature at 411 nm for the Y122• in *E. coli* R2. The sharpness of the latter has been exploited to spectrophotometrically determine [Y122•] in both kinetic and endpoint experiments. The "drop-line corrected" absorbance at 411 nm ($A_{411} - (A_{405} + A_{417})/2$), which effectively measures the height of the 411 nm peak, has been shown to be directly proportional to the concentration of Y122•. Despite the greater breadth of the 416 nm feature of the Y177• in mouse R2, the peak is still sufficiently sharp to allow for the application of the drop-line treatment. It was verified for a series of reconstituted mouse R2 samples having different concentrations of Y177• that $A_{416} - (A_{410} + A_{422})/2$ is directly proportional to the concentration of Y177• determined [as previously described (*15*)] directly by EPR spectroscopy (Figure S1). The proportionality constant (463 ± 20 M^{-1} cm^{-1}) provides an effective molar absorptivity ($\epsilon_{416} - (\epsilon_{410} - \epsilon_{422})/2$) to quantify Y177• directly from absorption spectra. This effective molar absorptivity is less than the corresponding value for the Y122 radical in *E. coli* R2, because the feature of the latter is much sharper. In addition, the precise value

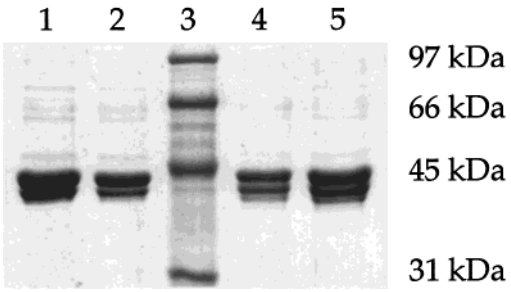

FIGURE 1: SDS−PAGE analysis of preparations of mouse R2 and R2−Y177F. Two different quantities of each preparation were resolved on a 12% polyacrylamide gel, and the gel was stained with coomassie brilliant blue. Lanes 1 and 2 are of R2−Y177F, with lane 1 having twice as much protein. Lanes 4 and 5 are of the wild-type protein, with lane 5 having twice as much protein. Lane 3 is of molecular weight standards (from the top down: 97, 66, 45, and 31 kDa).

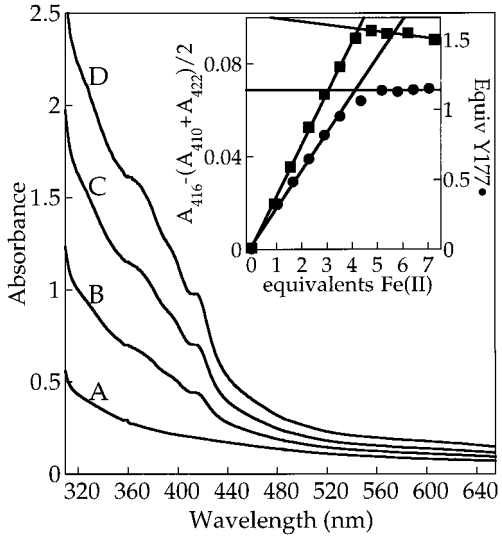

FIGURE 2: Spectrophotometrically monitored titration of apo mouse R2 with Fe(II) in the presence of O_2. The titration was carried out as described in Materials and Methods. The spectra shown were acquired after addition of (A) 0, (B) 1.0, (C) 2.3, and (D) 3.5 equiv Fe(II) relative to the R2 dimer (concentration of 0.14 mM). The inset shows plots of $A_{416} - (A_{410} + A_{422})/2$ and equiv Y177• versus equiv Fe(II) added in the presence (■) and absence (●) of 2.5 mM sodium ascorbate.

Scheme 2: Proposed mechanism of cofactor assembly in the R2 subunit of ribonucleotide reductase from mouse.

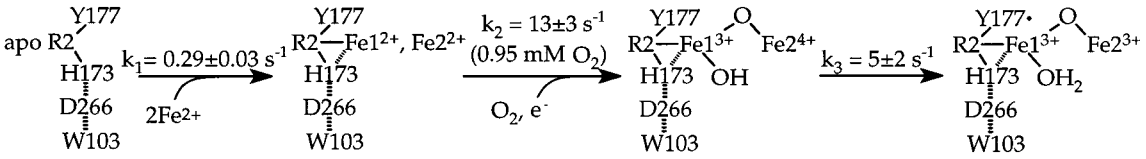

of $\epsilon_{416} - (\epsilon_{410} - \epsilon_{422})/2$ for the Y177• is sensitive to the wavelength calibration and spectral resolution of the spectrometer used.

Plots of $A_{416} - (A_{410} + A_{422})/2$ versus equiv Fe(II) added during titration of the apo protein at room temperature (inset to Figure 2) reveal that 4.2 ± 0.2 equiv of Fe(II) are needed for the production of the maximum quantity of Y177• (circular points). This equivalence point is not significantly different when 2.5 mM sodium ascorbate is included in the titration (square points). Therefore, the equivalence point most likely represents the stoichiometry of competent Fe sites. Support for this conclusion is provided by the Mössbauer spectrum of a product sample prepared by addition of 4.0 equiv of ^{57}Fe(II) to a solution of apo protein and ascorbate followed by addition of excess O_2 (Figure S2, Supporting Information). Component analysis of the spectrum indicates that >95% of the Fe absorption (corresponding to >3.8 equiv) is contributed by the features of the μ-(oxo)diiron-(III) cluster. Thus, in comparison with the situation for *E. coli* R2, which is generally observed to incorporate only 70−85% of its theoretical complement of four Fe ions per dimeric subunit, the Fe/R2 stoichiometry of mouse R2 appears to be more similar to its theoretical maximum. The maximum Y177•/R2 stoichiometry, 1.6 equiv per dimeric subunit in the presence of ascorbate, is also more similar to its theoretical value (2) than is observed for *E. coli* R2 (1.2 ± 0.1). These stoichiometries are similar to those previously reported by Thelander and co-workers (*27*, *29*). As previously noted, the greater Fe(II)/Y177• stoichiometry of the reaction in the absence of ascorbate reflects the need for the extra reducing equivalent (*9*, *15*, *30*). Ascorbate can provide this electron, whereas, in the absence of the reductant, a third Fe(II) is oxidized sacrificially to provide the electron for a diiron(II) cluster that reacts with O_2 (*9*, *15*, *30*). The measured Fe(II)/Y177• stoichiometries in the presence and absence of ascorbate (2.5 ± 0.3 and 3.4 ± 0.4) are quite similar to the theoretical minimum values of 2 and 3. It is noteworthy that the primary manifestation of the sacrificial oxidation of a fraction (theoretically, one-third) of the Fe(II) is a 1.3−1.4-fold decrease in the final Y177•/R2 stoichiometry of the product rather than a 1.5-fold increase in the quantity of Fe(II) needed to reach the same final Y177•/R2 stoichiometry.

Kinetics and Mechanism of the Mouse R2 Reaction by Stopped-Flow Absorption and Freeze-Quench EPR and Mössbauer Spectroscopies. Kinetic and spectroscopic data obtained by the three complementary methods are all consistent with the mechanism depicted in Scheme 2. The slowest step in the reaction ($k_{obs} = 0.29 \pm 0.03$ s^{-1} at 5 °C) is the first step, acquisition of Fe(II) by the apo protein to form the reactive Fe(II)−R2 complex. As in the reaction of *E. coli* R2 (*15*), this step has kinetic characteristics of a unimolecular change by the protein as long as Fe(II) is in excess or nearly in excess (Fe(II)/R2 ≥ 4.0). In other words, under these conditions, the reaction rate is independent of [Fe(II)]. Because this first step is much slower than subsequent steps leading to product, oxidized diiron intermediates do not accumulate significantly when the reaction is initiated by mixing of Fe(II) and apo R2. However, as in the reaction of *E. coli* R2 (*7*, *16*), formation of the reactive complex by incubation of apo R2 and Fe(II) in the absence of O_2 prior to initiation of the reaction by mixing with O_2 allows subsequent chemical steps to be unmasked and directly interrogated. Upon mixing of the preformed reactive complex with O_2 (final concentration 0.95 mM), the mouse R2 cognate of cluster X forms with an apparent first-order rate constant of 13 ± 3 s^{-1}. (The true kinetic order of this step has not yet been determined, and it is not clear whether or what intermediates may accumulate on the pathway leading to X.) The intermediate state containing X converts to the final Y177• and μ-(oxo)diiron(III)-containing product with a rate constant of 5 ± 2 s^{-1}. The data establishing that this scheme is operant are summarized as follows.

From time-dependent absorption spectra following mixing at 5 °C of apo R2 and excess Fe(II) (4−6 equiv) in the presence of 0.95 mM O_2 (Figure 3a), it would appear that the reaction is kinetically simple. Throughout the spectral range, absorbance values increase monotonically with uniform kinetics. Timecourses of $A_{416} - (A_{410} - A_{422})/2$ from the experiment of Figure 3a (inset) and five similar experiments could be analyzed as single-exponential growths with a mean (± standard deviation (SD)) apparent first-order rate constant of 0.27 ± 0.03 s^{-1} (dotted trace in inset). Evidence below indicates, however, that the reaction consists of a minimum of three kinetically significant steps (Scheme 2). Simulation of the traces according to Scheme 2 (solid line in Figure 3a inset) reproduces the detectable lag phase in the traces and, thus, gives better agreement with the data in the early part of the reaction. The fact that the lag phase is detectable indicates that, as expected from the magnitude of the rate constants, the faster chemical steps are not entirely kinetically masked by the slower complexation step.

In the lone experiment that was performed with Fe(II) decidedly limiting (2.5 equiv), a significantly lower value of k_{obs} (0.16 s^{-1}) was obtained. The sensitivity of k_{obs} to Fe(II)/R2 ratio in the limiting Fe(II) regime is consistent with rate-limitation by some step involved in the formation of the O_2-reactive diiron(II) cluster.

In contrast to the apparent kinetic simplicity of the Fe(II)-initiated reaction, the reaction as carried out by prior incubation of Fe(II) and apo R2 and initiation with O_2 (Figure 3b) exhibits three kinetic phases (inset); a lag phase in Y177• formation is followed by two well-resolved formation phases. The lag phase in these traces is attributable to the relatively rapid accumulation of an intermediate in the fraction of the R2 reactant that was converted into the reactive Fe(II)−R2 complex in the anoxic preincubation with Fe(II). The faster formation phase reflects conversion of the intermediate in this fraction of the protein into the Y177• and μ-(oxo)diiron-

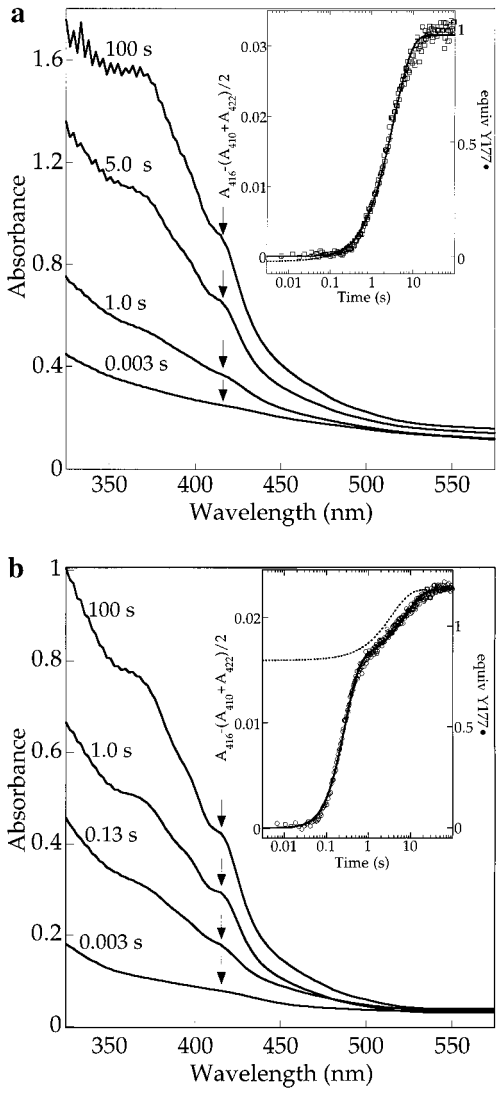

FIGURE 3: Development of the absorption spectrum of native mouse R2 at 5 °C after equal-volume mixing of (A) an O_2-free solution of 0.26 mM apo R2 in buffer C (see text) with an O_2-saturated solution of 1.53 mM Fe(II) (6 equiv) in 2.5 mM H_2SO_4 and (B) an O_2-free solution of 0.75 mM R2 and 3.3 mM Fe(II) (4.4. equiv) in buffer C with an O_2-saturated solution of buffer C. In both cases, the final $[O_2]$ should have been 0.95 mM. The path-length in A was 1 cm, whereas that in B was 0.2 cm. The insets show the kinetics of Y177• formation as reported by $A_{416} - (A_{410} + A_{422})/2$. In A, simulations of a simple first-order growth with rate-constant 0.27 s^{-1} and amplitude corresponding to 1 equiv Y177• (dotted line) and of the kinetics of Y177• formation predicted by Scheme 2 (solid line) are plotted over the data. In B, a simulation of the kinetics of Y177• according to Scheme 2 and the parameters given in the text is plotted over the data. The dashed trace in B is the fit from A, scaled for comparison to the slow phase of Y177• formation.

(III)-containing product. The slow phase is attributable to Y177• formation in that fraction of the protein that was not in the reactive form (presumably because at least one site of the diiron cluster remained unoccupied) upon initiation of the reaction with O_2 but is subsequently converted into the reactive form and thereupon reacts with O_2 to give the intermediate and then product. These traces (with the right-hand *y* axis, equivalents of Y177•, considered) can be analyzed according to eq 1, which describes the kinetics of Y177• formation according to Scheme 2 where $([Y177•]/[R2])_t$ is the stoichiometry of Y177• radical at any time, $([Y177•]/[R2])_\infty$ is the stoichiometry of Y177• radical at completion, $F_{unreactive}$ is the fraction of the R2 reactant not in the reactive form upon mixing with O_2, $F_{reactive}$ is the fraction in the reactive form, the rate constants k_1-k_3 are as defined in Scheme 2, and k_{23} is equal to $k_2k_3/(k_2 + k_3)$.[2] The fitting of this equation to the trace in Figure 3b and those from five similar experiments yielded apparent first-order rate constants of 13 ± 3 s^{-1} (mean ± SD) for reaction of the reactive Fe(II)−R2 complex with O_2, 4.7 ± 0.5 s^{-1} for decay of the intermediate and formation of Y177•, and 0.18 ± 0.08 s^{-1} for the slow acquisition of additional Fe(II) to convert the unreactive fraction of R2 into the reactive complex. In each of these experiments, which had Fe(II)/R2 ratios varying from 4.0 to 6.3 and R2 concentrations ranging from 0.12 to 0.38 mM, the fast formation phase accounted for 52−70% of the total Y177• produced, which varied from 0.8 to 1.2 equiv. Thus, in all six experiments, 0.42−0.84 equiv of Y177• formed in the phase with rate constant ∼5 s^{-1}. This rate constant is ∼16-fold greater than that established previously for the Fe(II)-initiated reaction. The fact that the majority of the Y177• forms more rapidly in the O_2-initiated case confirms that formation of the reactive Fe(II)−R2 complex rate-limits Y177• formation in the Fe(II)-initiated case. A similar situation exists in the *E. coli* R2 reaction: formation of the reactive Fe(II)−R2 complex (Scheme 1, step A) is also slower than the ensuing steps in which oxidized intermediates are formed (steps B, C) (*16*). A notable difference is that, in the *E. coli* R2 reaction, formation of the complex is slightly faster (5−10-fold) than the final radical-producing step (E) (*15*), whereas in the mouse R2 reaction, formation of the complex is ∼20-fold slower than the tyrosyl-radical-producing step. Thus, Y177• formation in mouse R2 could be accelerated in vivo by accessory factors (e.g., metallochaperones) that facilitate formation of the reactive Fe(II)−R2 complex, whereas the *E. coli* R2 reaction is rate-limited by a later step.

$$\left(\frac{[Y177•]}{[R2]}\right)_t = F_{unreactive}\left(\frac{[Y177•]}{[R2]}\right)_\infty (1 + (k_1 e^{-k_{23}t} - k_{23}e^{-k_1 t})/(k_{23} - k_1)) + F_{reactive}\left(\frac{[Y177•]}{[R2]}\right)_\infty (1 + (k_2 e^{-k_3 t} - k_3 e^{-k_2 t})/(k_3 - k_2)) \quad (1)$$

The apparent first-order rate constant for the slower phase of Y177• formation in the O_2-initiated reaction is dependent on the initial Fe(II)/R2 ratio, with the minimum ratio examined, 4, giving the minimum k_{obs} of 0.1 s^{-1}. With Fe(II) well in excess (6.3 equiv), a rate constant of 0.24 ±

[2] This latter term is essentially a net rate-constant for the two faster steps (those associated with k_2 and k_3) in the three-step sequence required to convert the fraction of R2 not initially in the reactive Fe(II)−R2 complex into product (Scheme 2). The approximation of the three-step sequence as a two-step sequence makes possible an analytical expression for Y177• production in the slow phase (the first term in eq 1), which, when added to the simpler expression for Y177• formation in the *actual* two-step sequence associated with the faster phase (the second term in eq 1), allows the data to be analyzed by nonlinear regression. Because the flux through the three-step sequence of the slower phase is almost entirely rate-limited by the first step, this approximation is essentially perfect. This conclusion was verified by simulation (with KinTekSim, KinTek Corporation, Austin, TX) of traces according to Scheme 2, with rate constants derived from the regression analysis, and comparison of these traces to those predicted by eq 1.

0.03 s^{-1} was obtained for this phase. The similarity of this value to that characterizing Y177• formation in the Fe(II)-initiated reaction supports the hypothesis that the slower phase reflects conversion of a fraction of the protein into the reactive Fe(II)−R2 complex by uptake of Fe(II). The incomplete conversion to reactive complex in the preincubation step is most simply rationalized by less-than-tight binding under the conditions employed. In this scenario, greater ratios of Fe(II)/R2 or higher concentrations of both at a constant ratio should be associated with smaller fractional amplitudes in the slow phase. Indeed, the experiments with the maximum Fe(II)/R2 ratio examined (6.3, with an R2 concentration of 0.15 mM) and the maximum concentration of R2 examined (0.37 mM with 4.4 equiv Fe(II)) gave the minimum slow-phase amplitudes (33% and 30% of the total amplitudes, respectively). Rigorous testing of this rationale for the slow phase will require more extensive variation of concentrations and ratio, elucidation of the effects on the relative amplitudes of the fast and slow phases, and direct interrogation of Fe(II) binding. In the absence of such direct evidence, other explanations for the slow phase (e.g., different kinetic behavior by that fraction of the protein that has undergone partial proteolysis or linkage between monomers of the dimeric protein) are also possible.

The lag phase preceding Y177• formation in the O_2-initiated reaction indicates that an intermediate species accumulates. As noted previously, two demonstrated intermediate states in the reaction of *E. coli* R2 both contain the formally Fe(III)Fe(IV) cluster X (Scheme 1), which exhibits a sharp, isotropic $g = 2.0$ EPR singlet and a distinctive paramagnetic Mössbauer signature (*5*, *7*, *15*, *17*−*19*, *24*). A species with a similar EPR signal has been detected in the reaction of the Y177F variant of mouse R2 (*12*) and, under one set of conditions, in the reaction of wild-type mouse R2 (*11*). In the latter case, however, the authors' analysis of the kinetics of formation and decay of this species led them to conclude that it was not an intermediate in Y177• formation. To test for accumulation of X during the lag phase preceding Y177• formation, freeze-quench EPR and Mössbauer experiments were performed. The development of total EPR intensity in the $g = 2.0$ region ("spin") exhibits two well-resolved kinetic phases with approximately equal amplitudes (Figure 4, circular points). The fast phase of spin development correlates well with the lag phase preceding Y177• formation detected in the stopped-flow experiments, and the slow phase correlates with the slow phase of Y177• radical formation. The solid line through the data represents a simulation according to Scheme 2 with $k_1 = 0.3$ s^{-1}, $k_2 = 12$ s^{-1}, 50% of the reactant initially in the reactive Fe(II)−R2 complex, and a final Y177• stoichiometry of 1.08 equiv. The EPR spectrum of a sample quenched during the rapid phase of spin development (Figure 5, spectrum A) has a very different line shape from that characteristic of the product radical, Y177• (spectrum D). This observation indicates that an additional $g \sim 2.0$ EPR active species (X) accumulates during this fast phase and decays as Y177• is formed. In kinetic studies of the *E. coli* R2 reaction, time-dependent EPR spectra of samples containing both X and Y122• have been analyzed by iterative summation of reference spectra for the two species, with varying intensity-weighting factors, until each experimental spectrum is reproduced (*15*, *16*). From the fractions of X and Y122• indicated by the reconstruction of a given spectrum and the total spin reflected by that spectrum, the concentration of each species is calculated. The reference spectrum for X is from a freeze-quenched sample of the Y122F variant protein. With the intermediate's target for oxidation (Y122) replaced with the less easily oxidized residue (F), X has a ∼5-fold greater lifetime and is the vastly predominant $g \sim 2.0$ EPR active species at reaction times of less than a second (*5*, *15*). The lifetime-enhancing effect on mouse X of the corresponding Y177F substitution in mouse R2 also has recently been demonstrated (*12*). Therefore, a similar approach was employed for analysis of the spectra of Figure 5. A sample prepared by incubation of apo R2−Y177F with Fe(II) (4 equiv), initiation of the reaction by mixing at 11 °C with O_2-saturated buffer, and freeze-quenching after 0.35 s reaction time exhibits an isotropic $g = 2.0$ singlet (Figure 5, spectrum E) essentially identical with that characteristic of X in the *E. coli* R2 reaction (*5*, *17*, *18*) and that previously reported for mouse X in the Y177F variant (*12*). This spectrum was taken as a reference for the mouse R2 X intermediate. Intensity weighted summations of this spectrum with that of the freeze-quenched Y177• product of the wild-type R2 reaction (spectrum D) satisfactorily reproduce the experimental time-dependent spectra (Figure 5, spectra A′−

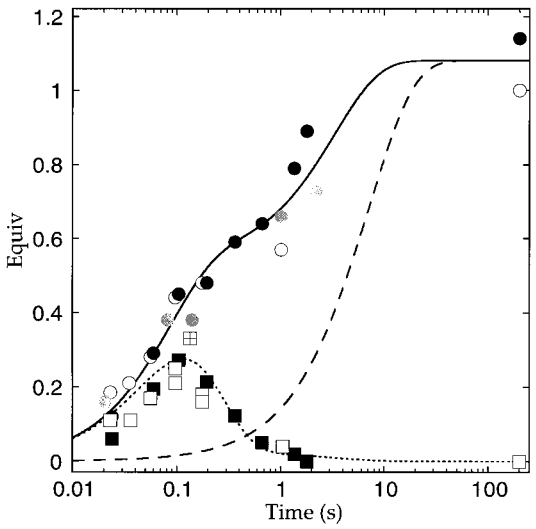

FIGURE 4: Kinetics by freeze-quench EPR of development of total "spin" (circular points) and of formation and decay of intermediate X (square points) after mixing at 5 °C of an O_2-free solution of R2 and Fe(II) in buffer C with O_2-saturated buffer C. The data for total spin are from three separate experiments. The concentrations after mixing were as follows: experiment 1 (black filled circles), [R2] = 0.17 mM, [Fe(II)] = 1.1 mM (6.3 equiv), [O_2] = 1.3 mM; experiment 2 (gray filled circles), [R2] = 0.15 mM, [Fe(II)] = 0.77 mM (5.0 equiv), [O_2] = 1.3 mM; experiment 3 (open circles), [R2] = 0.20 mM, [Fe(II)] = 0.79 mM (4.0 equiv), [O_2] = 0.95 mM. The data for X were obtained by deconvolution (as described in the text) of experimental spectra from experiments 1 and 3 (black filled squares and open squares, respectively). In experiment 3, duplicate samples were prepared for two of the reaction times (0.097 and 0.18 s). The average total spin for each pair is plotted, but the quantity of X determined for each sample is plotted separately. The quantity of X deduced by analysis of the Mössbauer spectrum of the 0.135 s sample is also shown (square point with cross). The solid and dotted traces plotted over the data are simulations, according to Scheme 2 and to parameters given in the text, of the kinetics of total spin (X + Y177•) and X, respectively. The dashed trace is a simulation of Y177• formation according to the parameters given by Schmidt et al. (*11*). Details of spectral acquisition and analysis are given in the legend to Figure 5.

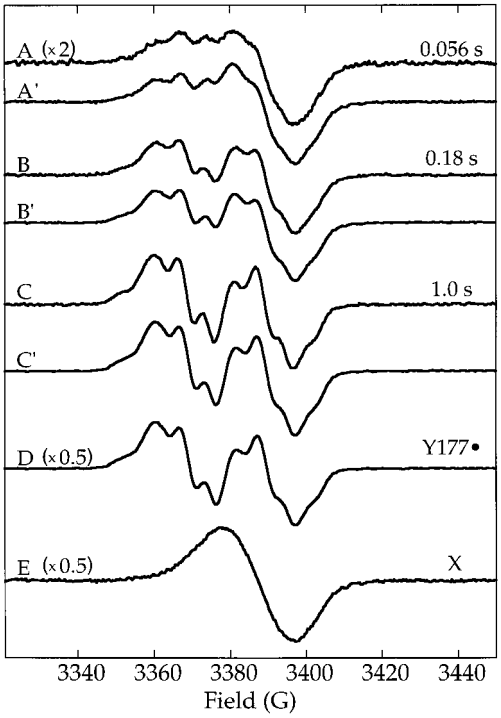

FIGURE 5: Component analysis of EPR spectra obtained in experiment 3 of Figure 4. In each of the first three pairs of spectra, the upper spectrum (labeled A, B, or C) is of the sample freeze-quenched at the indicated reaction time, and the lower spectrum (labeled A′, B′, or C′) is the corresponding reconstruction by summation of the reference spectra for Y177• (spectrum D) and X (spectrum E). Spectrum D is of the 200 s sample from experiment 3. Spectrum E is of a sample obtained by equal-volume mixing at 11 °C of an O_2-free solution of 0.30 mM apo R2−Y177F and 1.2 mM Fe(II) in buffer C with O_2-saturated buffer C and freeze-quenching at a reaction time of 0.35 s. All spectra were recorded at 20 K with a microwave power of 6.3 μW and a modulation amplitude of 4 G. For A−D, a scan time of 160 s and a time constant of 0.16 s were used. For E, the scan time was increased to 1300 s and the time constant to 1.3 s. Integrated spectral intensities were related to concentration by use of a copper perchlorate standard, as previously described (*15*).

C′). The quantities of X (filled and open squares in Figure 4) deduced from the intensity-weighting factors for optimal reconstruction and the integrated $g = 2.0$ intensities of the spectra from two separate experiments are consistent with those predicted by Scheme 2. The dotted line in Figure 4 is a simulation according to Scheme 2 with the same parameters used to generate the solid trace ($k_1 = 0.3$ s^{-1}, $k_2 = 12$ s^{-1}, $[Y177•/R2]_{final} = 1.08$, 50% of the reactant initially in the reactive Fe(II)−R2 complex) and $k_3 = 6.5$ s^{-1}. Given the considerable uncertainty associated with EPR spin quantitation in general and with this sort of spectral deconvolution in particular, we consider the agreement of this value for k_3 with that extracted by analysis of the stopped-flow data 4.7 ± 0.5 s^{-1} to be acceptable. In addition, we judge the agreement of the fraction of R2 initially in the reactive Fe(II)−R2 complex (50%) assumed in the analysis of Figure 4 with that deduced from analysis of stopped-flow data acquired under similar reaction conditions (52−70%) also to be acceptable.

To obtain more definitive evidence for the accumulation of cluster X in the lag phase preceding Y177• formation, a series of freeze-quenched Mössbauer samples were prepared and analyzed. A paramagnetic signature very similar to that

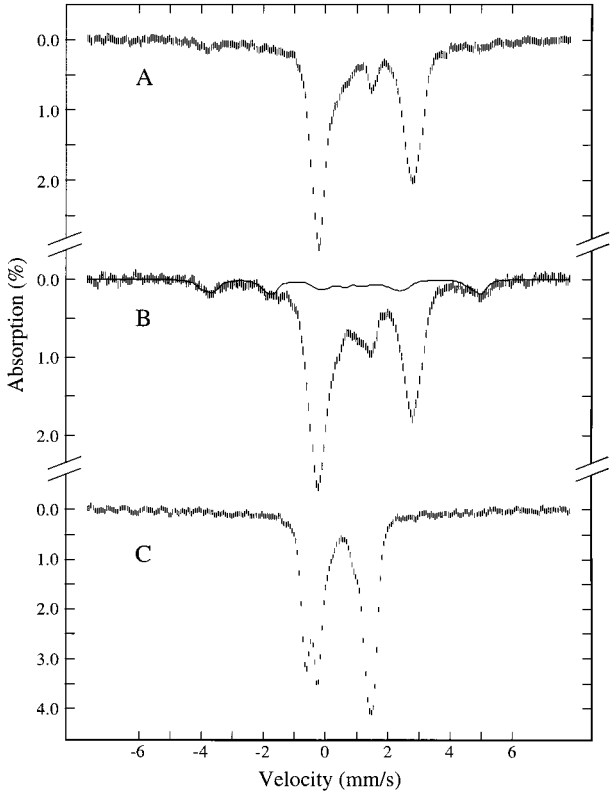

FIGURE 6: Mössbauer spectra of samples prepared by equal-volume mixing at 5 °C of an O_2-free solution of 0.75 mM R2 and 3.3 mM ^{57}Fe(II) with an O_2-saturated solution of buffer C and freeze-quenching after (A) 0.023 s, (B) 0.135 s, or (C) 200 s. The data (hashed marks) were recorded at 4.2 K in a parallel applied field of 50 mT. The solid line in B is the theoretical spectrum of X in *E. coli* R2 simulated with the published parameters (*19*). The theoretical spectrum is scaled to 15% of the total Fe absorption of the experimental spectrum.

characterizing X from the *E. coli* R2 reaction (*17*−*19*) is most prominent in the spectrum of a sample that was freeze-quenched at a reaction time of 0.135 s (Figure 6, spectrum B), which is similar to the time at which the concentration of the intermediate is predicted by Scheme 2 to reach its maximum value (with the assumption that approximately half of the R2 begins in the reactive complex). The spectrum of a sample quenched at a shorter reaction time (0.023 s, spectrum A) has less intensity attributable to X, and the features are undetectable in the spectrum of a sample freeze-quenched after completion (200 s, spectrum C). With the simplest assumption that the spectrum of mouse X is identical with that of *E. coli* X, a contribution of 15 ± 3% of the total Fe absorption is estimated for the 0.135 s sample (solid line plotted over spectrum B). This corresponds to 0.33 ± 0.07 equiv of X (square point with cross in Figure 4), which is in satisfactory agreement both with the quantity of X estimated in analysis of the EPR spectra and with the quantity predicted by the simulation.

The combined stopped-flow absorption and freeze-quench EPR and Mössbauer data provide strong evidence that cluster X is an intermediate on the pathway to the Y177• and μ-(oxo)diiron(III) cluster of the native mouse R2 protein. The intermediate accumulates to ∼0.3 equiv with an observed first-order rate constant (with 0.95 mM O_2) of 13 ± 3 s^{-1} and decays as Y177• forms with a rate constant of 5 ± 2 s^{-1}. Given that transfer of the extra reducing equivalent

to the cluster must occur in formation of X, a lower limit of $\sim 10\ s^{-1}$ may be set for the rate constant of this step. Thus, it is clear that this step is not primarily rate-limiting in formation of Y177• under any conditions and not at all rate-limiting in starting from the apo protein and Fe(II).

The principal findings of this study (the kinetic competence of mouse X for production of Y177• and the overall rate-limitation by formation of the reactive Fe(II)−R2 complex rather than by the transfer of the extra reducing equivalent associated with formation of X) are inconsistent with the conclusions of Schmidt et al. (*11*). These authors reported slow formation of Y177• ($k_{obs} = 0.14 \pm 0.03\ s^{-1}$, dashed trace in Figure 4) in both the Fe(II)-initiated and the O_2-initiated reactions and little or no accumulation of X in either case. The simplest explanation for these discrepancies is that the reactive Fe(II)−R2 complex did not form to a significant extent under the preincubation conditions employed by Schmidt et al. The X-ray crystallographic results of Kauppi et al. (*31*), who observed that the Fe1 site was vacant and the Fe2 site only partially occupied in crystals of mouse R2 at pH 4.7 and that the Fe1 site did not retain Fe(II) upon its infusion into the crystals, and our inference that the conversion of apo R2 into the reactive complex is incomplete even after preincubation with ≥6 equiv Fe(II) suggest that Fe(II) binding by mouse R2 may be sufficiently weak as to be sensitive to relatively minor differences in the conditions used in the preincubation step. Most likely, the inclusion by Schmidt et al. (*11*) of 0.1 M potassium chloride and a relatively high concentration (0.1 M) of a basic buffer (Tris) at a pH (7.5) well below its pK_a resulted in an ionic strength sufficiently high to attenuate the primarily ionic binding interaction between the protein and Fe(II) ions. This ionic shielding effect could also explain the ∼2.5-fold slower formation of the complex (which, in the present scenario, would have been exclusively rate-limiting for the first-order formation of Y177•) observed by these authors. A second possibility is that the 10% glycerol included in our experiments but not in those of Schmidt et al. favors formation of the reactive Fe(II)−R2 complex. A "chemical chaperone" activity of glycerol has been noted (*32*, *33*), but we are unaware of any report of a *metallo*chaperone-like effect of this molecule. Experiments to test these explanations are in progress.

The possibility remains that the transfer of the extra reducing equivalent is rate-limiting for formation of X in the mouse R2 reaction. In this case, an intermediate one electron more oxidized than X should accumulate. The precursor to X in the reaction of *E. coli* R2 has been an elusive quarry due to its very rapid reductive trapping by W48 (*7*). Given the kinetic differences demonstrated herein, it is not unreasonable to hope that further investigation of the mouse R2 reaction may yield insight into these early steps that are kinetically masked in the *E. coli* R2 reaction.

SUPPORTING INFORMATION AVAILABLE

Figure S1, showing determination of the drop-line corrected molar absorptivity [$\epsilon_{416} - (\epsilon_{410} + \epsilon_{422})/2$] of Y177•, and Figure S2, showing the Mössbauer spectrum of mouse R2 reconstituted in the presence of 2.5 mM ascorbate with 4.0 equiv ^{57}Fe. This material is available free of charge via the Internet at http://pubs.acs.org.

REFERENCES

1. Nordlund, P., Sjöberg, B.-M., and Eklund, H. (1990) *Nature 345*, 593−598.
2. Nordlund, P., and Eklund, H. (1993) *J. Mol. Biol. 232*, 123−164.
3. Stubbe, J., and Riggs-Gelasco, P. (1998) *Trends Biochem. Sci. 23*, 438−443.
4. Atkin, C. L., Thelander, L., Reichard, P., and Lang, G. (1973) *J. Biol. Chem. 248*, 7464−7472.
5. Bollinger, J. M., Jr., Edmondson, D. E., Huynh, B. H., Filley, J., Norton, J. R., and Stubbe, J. (1991) *Science 253*, 292−298.
6. Bollinger, J. M., Jr., Tong, W. H., Ravi, N., Huynh, B. H., Edmondson, D. E., and Stubbe, J. (1995) *Methods Enzymol. 258*, 278−303.
7. Baldwin, J., Krebs, C., Ley, B. A., Edmondson, D. E., Huynh, B. H., and Bollinger, J. M., Jr. (2000) *J. Am. Chem. Soc. 122*, 12195−12206.
8. Krebs, C., Chen, S., Baldwin, J., Ley, B. A., Patel, U., Edmondson, D. E., Huynh, B. H., and Bollinger, J. M., Jr. (2000) *J. Am. Chem. Soc. 122*, 12207−12219.
9. Ochiai, E., Mann, G. J., Gräslund, A., and Thelander, L. (1990) *J. Biol. Chem. 265*, 15758−15761.
10. Rova, U., Goodtzova, K., Ingemarson, R., Behravan, G., Gräslund, A., and Thelander, L. (1995) *Biochemistry 34*, 4267−4275.
11. Schmidt, P. P., Rova, U., Katterle, B., Thelander, L., and Gräslund, A. (1998) *J. Biol. Chem. 273*, 21463−21472.
12. Pötsch, S., Lendzian, F., Ingemarson, R., Hörnberg, A., Thelander, L., Lubitz, W., Lassmann, G., and Gräslund, A. (1999) *J. Biol. Chem. 274*, 17696−17704.
13. Nguyen, H.-H. T., Ge, J., Perlstein, D. L., and Stubbe, J. (1999) *Proc. Natl. Acad. Sci. U.S.A. 96*, 12339−12344.
14. Ge, J., Perlstein, D. L., Nguyen, H.-H., Bar, G., Griffin, R. C., and Stubbe, J. (2001) *Proc. Natl. Acad. Sci. U.S.A. 98*, 10067−10072.
15. Bollinger, J. M., Jr., Tong, W. H., Ravi, N., Huynh, B. H., Edmondson, D. E., and Stubbe, J. (1994) *J. Am. Chem. Soc. 116*, 8015−8023.
16. Tong, W. H., Chen, S., Lloyd, S. G., Edmondson, D. E., Huynh, B. H., and Stubbe, J. (1996) *J. Am. Chem. Soc. 118*, 2107−2108.
17. Bollinger, J. M., Jr., Stubbe, J., Huynh, B. H., and Edmondson, D. E. (1991) *J. Am. Chem. Soc. 113*, 6289−6291.
18. Ravi, N., Bollinger, J. M., Jr., Huynh, B. H., Edmondson, D. E., and Stubbe, J. (1994) *J. Am. Chem. Soc. 116*, 8007−8014.
19. Sturgeon, B. E., Burdi, D., Chen, S., Huynh, B. H., Edmondson, D. E., Stubbe, J., and Hoffman, B. M. (1996) *J. Am. Chem. Soc. 118*, 7551−7557.
20. Burdi, D., Sturgeon, B. E., Tong, W. H., Stubbe, J., and Hoffman, B. M. (1996) *J. Am. Chem. Soc. 118*, 281−282.
21. Willems, J.-P., Lee, H.-I., Burdi, D., Doan, P. E., Stubbe, J., and Hoffman, B. M. (1997) *J. Am. Chem. Soc. 119*, 9816−9824.
22. Riggs-Gelasco, P. J., Shu, L., Chen, S., Burdi, D., Huynh, B. H., Que, L., Jr., and Stubbe, J. (1998) *J. Am. Chem. Soc. 120*, 849−860.
23. Burdi, D., Willems, J.-P., Riggs-Gelasco, P., Antholine, W. E., Stubbe, J., and Hoffman, B. M. (1998) *J. Am. Chem. Soc. 120*, 12910−12919.
24. Bollinger, J. M., Jr., Tong, W. H., Ravi, N., Huynh, B. H., Edmondson, D. E., and Stubbe, J. (1994) *J. Am. Chem. Soc. 116*, 8024−8032.
25. Thelander, M., and Thelander, L. (1989) *EMBO J. 8*, 2475−2479.
26. Kim, R., Sandler, S. J., Goldman, S., Yokota, H., Clark, A. J., and Kim, S. H. (1998) *Biotechnol. Lett. 20*, 207−210.
27. Mann, G. J., Graslund, A., Ochiai, E., Ingemarson, R., and Thelander, L. (1991) *Biochemistry 30*, 1939−1947.
28. Parkin, S. E., Chen, S., Ley, B. A., Mangravite, L., Edmondson, D. E., Huynh, B. H., and Bollinger, J. M., Jr. (1998) *Biochemistry 37*, 1124−1130.
29. Rova, U., Adrait, A., Potsch, S., Graslund, A., and Thelander, L. (1999) *J. Biol. Chem. 274*, 23746−23751.

30. Elgren, T. E., Lynch, J. B., Juarez-Garcia, C., Münck, E., Sjöberg, B.-M., and Que, L., Jr. (1991) *J. Biol. Chem. 266*, 19265−19268.
31. Kauppi, B., Nielsen, B. B., Ramaswamy, S., Kjøller-Larson, I., Thelander, M., Thelander, L., and Eklund, H. (1996) *J. Mol. Biol. 262*, 706−720.
32. Raibekas, A. A., and Massey, V. (1996) *Proc. Natl. Acad. Sci. U.S.A. 93*, 7546−7551.
33. Raibekas, A. A., and Massey, V. (1997) *J. Biol. Chem. 272*, 22248−22252.

BI011797P